Article

Ruthenium Nanoparticles inside Porous [Zn O(bdc)] by Hydrogenolysis of Adsorbed [Ru(cod)(cot)]: A Solid-State Reference System for Surfactant-Stabilized Ruthenium Colloids

Felicitas Schröder, Daniel Esken, Mirza Cokoja, Maurits W. E. van den Berg, Oleg I. Lebedev, Gustaaf Van Tendeloo, Bernadeta Walaszek, Gerd Buntkowsky, Hans-Heinrich Limbach, Bruno Chaudret, and Roland A. Fischer

J. Am. Chem. Soc., **2008**, 130 (19), 6119-6130 • DOI: 10.1021/ja078231u • Publication Date (Web): 11 April 2008

J|A|C|S
ARTICLES

Published on Web 04/11/2008

Ruthenium Nanoparticles inside Porous $[Zn_4O(bdc)_3]$ by Hydrogenolysis of Adsorbed [Ru(cod)(cot)]: A Solid-State Reference System for Surfactant-Stabilized Ruthenium Colloids

Felicitas Schröder,[†] Daniel Esken,[†] Mirza Cokoja,[†] Maurits W. E. van den Berg,[#] Oleg I. Lebedev,[‡] Gustaaf Van Tendeloo,[‡] Bernadeta Walaszek,[§] Gerd Buntkowsky,[§] Hans-Heinrich Limbach,[⊥] Bruno Chaudret,[||] and Roland A. Fischer*[,†]

Lehrstuhl für Anorganische Chemie II—Organometallics & Materials, and Lehrstuhl für Technische Chemie, Ruhr-Universität, Universitätsstrasse 150, D-44780 Bochum, Germany, EMAT, University of Antwerp, Groenenborgerlaan 171, B-2020 Antwerp, Belgium, Institut für Physikalische Chemie, Friedrich-Schiller-Universität, D-07743 Jena, Germany, Physikalische and Theoretische Chemie, Freie Universität, D-11195 Berlin, Germany, and Laboratoire de Chimie de Coordination—CNRS, F-31077 Toulouse Cedex 4, France

Received October 27, 2007; E-mail: roland.fischer@ruhr-uni-bochum.de

Abstract: The gas-phase loading of $[Zn_4O(bdc)_3]$ (MOF-5; bdc = 1,4-benzenedicarboxylate) with the volatile compound [Ru(cod)(cot)] (cod = 1,5-cyclooctadiene, cot = 1,3,5-cyclooctatriene) was followed by solid-state ^{13}C magic angle spinning (MAS) NMR spectroscopy. Subsequent hydrogenolysis of the adsorbed complex inside the porous structure of MOF-5 at 3 bar and 150 °C was performed, yielding ruthenium nanoparticles in a typical size range of 1.5–1.7 nm, embedded in the intact MOF-5 matrix, as confirmed by transmission electron microscopy (TEM), selected area electron diffraction (SAED), powder X-ray diffraction (PXRD), and X-ray absorption spectroscopy (XAS). The adsorption of CO molecules on the obtained Ru@MOF-5 nanocomposite was followed by IR spectroscopy. Solid-state ^2H NMR measurements indicated that MOF-5 was a stabilizing support with only weak interactions with the embedded particles, as deduced from the surprisingly high mobility of the surface Ru—D species in comparison to surfactant-stabilized colloidal Ru nanoparticles of similar sizes. Surprisingly, hydrogenolysis of the $[Ru(cod)(cot)]_{3.5}$@MOF-5 inclusion compound at the milder condition of 25 °C does not lead to the quantitative formation of Ru nanoparticles. Instead, formation of a ruthenium—cyclooctadiene complex with the arene moiety of the bdc linkers of the framework takes place, as revealed by ^{13}C MAS NMR, PXRD, and TEM.

Introduction

Starting from metal—organic coordination polymers developed by Robson et al.,[1,2] Yaghi and O'Keeffe[3,4] introduced the so-called metal—organic frameworks (MOFs) possessing inorganic parts with larger dimensionality as secondary building units. MOFs are an emerging family of materials with functional properties going far beyond zeolites and other ordered micro- and mesoporous inorganic compounds.[5,6] This is particularly true for the soft porous crystals, which are coordination polymers with a flexible framework responding to chemical and physical stimuli, developed by Kitagawa et al.[7,8] Also, the materials of Institute Lavoisier (MILs) investigated by Férey et al.,[9,10] with MIL-101 being the most porous material to date,[11] are very prominent examples among the many MOFs that have been studied. MOFs are highly interesting as advanced materials for gas storage and separation.[12] Many other applications are discussed, including chemical sensing,[13,14] drug-release,[15] photovoltaics,[16,17] and catalysis.[18–20] The embedding of functional nanoparticles inside the cavities of MOFs is relevant for

[†] Anorganische Chemie II, Ruhr-Universität.
[#] Technische Chemie, Ruhr-Universität.
[‡] EMAT, University of Antwerp.
[§] Physikalische Chemie, Friedrich-Schiller-Universität.
[⊥] Physikalische and Theoretische Chemie, Freie Universität.
[||] Laboratoire de Chimie de Coordination—CNRS.

(1) Hoskins, B. F.; Robson, R. *J. Am. Chem. Soc.* **1990**, *112*, 1546–1554.
(2) Stuart, R. S.; Robson, R. *Angew. Chem., Int. Ed.* **1998**, *37*, 1461–1494.
(3) Li, H.; Eddaoudi, M.; O'Keeffe, M.; Yaghi, M. *Nature* **1999**, *402*, 276–279.
(4) Yaghi, O. M.; O'Keeffe, M.; Ockwig, N. W.; Chae, H. K.; Eddaoudi, M.; Kim, J. *Nature* **2003**, *423*, 705–714.
(5) Ciesla, U.; Schuth, F. *Microporous Mesoporous Mater.* **1999**, *27*, 131–149.
(6) Cheetham, A. K.; Férey, G.; Loiseau, T. *Angew. Chem., Int. Ed.* **1999**, *38*, 3268–3292.
(7) Kitagawa, S.; Kitaura, R.; Noro, S.-i. *Angew. Chem., Int. Ed.* **2004**, *43*, 2334–2375.
(8) Kitagawa, S.; Uemura, K. *Chem. Soc. Rev.* **2005**, *34*, 109–119.
(9) Férey, G.; Mellot-Draznieks, C.; Serre, C.; Millange, F. *Acc. Chem. Res.* **2005**, *38*, 217–225.
(10) Férey, G. *Chem. Soc. Rev.* **2008**, *37*, 191–214.
(11) Férey, G.; Mellot-Draznieks, C.; Serre, C.; Millange, F.; Dutour, J.; Surble, S.; Margiolaki, I. *Science* **2005**, *309*, 2040–2042.
(12) Mueller, U.; Schubert, M.; Teich, F.; Puetter, H.; Schierle-Arndt, K.; Pastre, J. *J. Mater. Chem.* **2006**, *16*, 626–636.

a number of applications, including heterogeneous catalysis.[21] We and others have loaded $[Zn_4O(bdc)_3]$ (bdc = 1,4-benzenedicarboxylate; MOF-5 or IRMOF-1)[3] with Pd to yield Pd@MOF-5 materials, which revealed superior activity in olefin hydrogenolysis.[21,22] Similarly, Cu@MOF-5 showed surprising activity on methanol synthesis from CO and H_2.[21] The loading of MOFs with metal particles may be possible by the "incipient wetness" method, for example, by using a solution of $[Pd(acac)_2]$ (acac = acetylacetonate) in dichloromethane with subsequent drying and calcination/reduction with hydrogen, as recently demonstrated by Kaskel et al. for Pd@MOF-5 with about 1 wt % Pd loading.[22] Our group is focusing on solvent-free loading via adsorption from the gas phase using volatile all-hydrocarbon organometallic compounds known as precursors for metal−organic chemical vapor deposition (MOCVD), which allows a comparably high metal loading up to 30–40 wt % in a single loading step.[23] The isolable inclusion compounds of the type precursor@MOF are then converted into metal@MOF by thermally induced or photo-enhanced hydrogenolysis at 25 °C or below.[21] The method can conveniently be applied to the loading of MOF thin films with nanometals on various substrates, too.[24,25] In contrast to zeolites, mesoporous silica materials, and other porous solid-state support materials for nanoparticles, MOFs are chemically more labile, and the loading procedure may affect or even destroy the MOF structure. The interaction of the nanoparticle itself with the host matrix may range from rather weak to quite strong, obviously depending on the chemistry of the particle/MOF interfaces. We suggest conceptually viewing MOFs as some sort of solid solvent cage for this kind of host–guest chemistry. The organic linkers of the framework may play a role analogous to that of solvents and/or surfactants in nanoparticle colloid chemistry. In order to probe and develop this analogy, we selected the system Ru@MOF-5 as target and case study for the following reasons. First, ruthenium is a catalytically very interesting element. Organometallic ruthenium complexes are prominent in the homogeneous olefin methathesis.[26,27] Ba-promoted ruthenium supported on Al_2O_3 is interesting as a catalyst for ammonia synthesis.[28] Oxidation reactions of organic compounds can be catalyzed by Ru supported on zeolites,[29–32] and surfactant-stabilized ruthenium nanoparticles are very well known to be catalysts in hydrogenation reactions.[33,34] Such ruthenium colloids were obtained via the polyol process from $RuCl_3$[35,36] as well as by reduction with $NaBH_4$, as typical examples.[35] However, in terms of particle purity and perfect control over size and shape distribution by the surface chemistry, the apparently most successful preparation method is the hydrogenolysis of highly reactive all-hydrocarbon organometallic precursors, such as [Ru(cod)(cot)] (cod = 1,5-cyclooctadiene, cot = 1,3,5-cyclooctatriene).[37] All these liquid-phase routes to nanoparticles need suitable surfactants such as alkylamines, -thiols, -alcohols, or -silanes in the appropriate amounts to prevent particle agglomeration and to control the growth by adsorption to the particle surface. Alternatively, the growth can be limited by caging effects combined with particle−support interaction, as in the case of nano Ru inside porous silica and alumina membranes.[38,39] Obviously, MOFs offer a novel way of combining caging effects of porous solid-state matrices with surfactant/particle interaction in a very defined and molecularly controlled manner, extending the previously mentioned concepts and going beyond the embedding into pure organic polymers.[40] Thus, $[Zn_4O(bdc)_3]$ (MOF-5) is expected to stabilize very small Ru nanoparticles in the target system Ru@MOF-5 with a narrrow size distribution, possibly well below 2 nm, and revealing only weak interaction with the particle surface. In order to probe the surface chemistry of the caged Ru particles in relation to surfactant-stabilized nano Ru, we studied the mobility of chemisorbed hydrogen by temperature-dependent deuterium wide-line solid-state NMR and compared the data with those

(13) Bauer, C. A.; Timofeeva, T. V.; Settersten, T. B.; Patterson, B. D.; Liu, V. H.; Simmons, B. A.; Allendorf, M. D. *J. Am. Chem. Soc.* **2007**, *129*, 7136–7144.
(14) Chen, B.; Yang, Y.; Zapata, F.; Lin, G.; Qian, G.; Lobkovsky, E. B. *Adv. Mater.* **2007**, *19*, 1693–1696.
(15) Horcajada, P.; Serre, C.; Vallet-Regi, M.; Sebban, M.; Taulelle, F.; Férey, G. *Angew. Chem., Int. Ed.* **2006**, *45*, 5974–5978.
(16) Llabres i Xamena, F. X.; Corma, A.; Garcia, H. *J. Phys. Chem. C* **2007**, *111*, 80–85.
(17) Alvaro, M.; Carbonell, E.; Ferrer, B.; Llabres i Xamena, F. X.; Garcia, H. *Chem.-Eur. J.* **2007**, *13*, 5106–5112.
(18) Wu, C.-D.; Hu, A.; Zhang, L.; Lin, W. *J. Am. Chem. Soc.* **2005**, *127*, 8940–8941.
(19) Cho, S.-H.; Ma, B.; Nguyen, S. T.; Hupp, J. T.; Albrecht-Schmitt, T. E. *Chem. Commun.* **2006**, *24*, 2563–2565.
(20) Uemura, T.; Kitaura, R.; Ohta, Y.; Nagaoka, M.; Kitagawa, S. *Angew. Chem., Int. Ed.* **2006**, *45*, 4112–4116.
(21) Hermes, S.; Schroeter, M.-K.; Schmid, R.; Khodeir, L.; Muhler, M.; Tissler, A.; Fischer, R. W.; Fischer, R. A. *Angew. Chem., Int. Ed.* **2005**, *44*, 6237–6241.
(22) Sabo, M.; Henschel, A.; Froede, H.; Klemm, E.; Kaskel, S. *J. Mater. Chem.* **2007**, *17*, 3827–3832.
(23) Hermes, S.; Schroeder, F.; Amirjalayer, S.; Schmid, R.; Fischer, R. A. *J. Mater. Chem.* **2006**, *16*, 2464–2472.
(24) Hermes, S.; Schroeder, F.; Chelmowski, R.; Woell, C.; Fischer, R. A. *J. Am. Chem. Soc.* **2005**, *127*, 13744–13745.
(25) Hermes, S.; Zacher, D.; Baunemann, A.; Woell, C.; Fischer, R. A. *Chem. Mater.* **2007**, *19*, 2168–2173.
(26) Grubbs, R. H.; Tumas, W. *Science* **1989**, *243*, 907–915.
(27) Grubbs, R. H.; Chang, S. *Tetrahedron* **1998**, *54*, 4413–4450.
(28) Bielawa, H.; Hinrichsen, O.; Birkner, A.; Muhler, M. *Angew. Chem., Int. Ed.* **2001**, *40*, 1061–1063.
(29) Yamaguchi, K.; Mizuno, N. *Angew. Chem., Int. Ed.* **2002**, *41*, 4538–4542.
(30) Zhan, B.-Z.; White, M. A.; Sham, T.-K.; Pincock, J. A.; Doucet, R. J.; Rao, K. V. R.; Robertson, K. N.; Cameron, T. S. *J. Am. Chem. Soc.* **2003**, *125*, 2195–2199.
(31) Ho, C.-M.; Yu, W.-Y.; Che, C.-M. *Angew. Chem., Int. Ed.* **2004**, *43*, 3303–3307.
(32) Kim, W.-H.; Park, I. S.; Park, J. *Org. Lett.* **2006**, *8*, 2543–2545.
(33) Miao, S.; Liu, Z.; Han, B.; Huang, J.; Sun, Z.; Zhang, J.; Jiang, T. *Angew. Chem., Int. Ed.* **2005**, *45*, 266–269.
(34) (a) Kormann, H.-P.; Schmid, G.; Pelzer, K.; Philippot, K.; Chaudret, B. *Z. Anorg. Allgem. Chem.* **2004**, *630*, 1913–1918. (b) Jansat, S.; Picurelli, D.; Pelzer, K.; Philippot, K.; Gomez, M.; Muller, G.; Lecante, P.; Chaudret, B. *New J. Chem.* **2006**, *30*, 115–122. (c) Garcia Anton, J.; Axet, M. R.; Jansat, S.; Philippot, K.; Chaudret, B.; Pery, T.; Buntkowsky, G.; Limbach, H.-H. *Angew. Chem.* **2008**, *11*, 2074.
(35) Boennemann, H.; Brijoux, W.; Brinkmann, R.; Dinjus, E.; Joussen, T.; Korall, B. *Angew. Chem., Int. Ed.* **1991**, *10*, 1312–1314.
(36) Viau, G.; Brayner, R.; Poul, L.; Chakroune, N.; Lacaze, E.; Fievet-Vincent, F.; Fievet, F. *Chem. Mater.* **2003**, *15*, 486–494.
(37) (a) Pan, C.; Pelzer, K.; Philippot, K.; Chaudret, B.; Dassenoy, F.; Lecante, P.; Casanove, M.-J. *J. Am. Chem. Soc.* **2001**, *123*, 7584–7593. (b) Pelzer, K.; Laleu, B.; Lefebvre, F.; Philippot, K.; Chaudret, B.; Candy, J. P.; Basset, J. M. *Chem. Mater.* **2004**, *16*, 4937–4941. (c) Pelzer, K.; Vidoni, O.; Philippot, K.; Chaudret, B.; Colliere, V. *Adv. Funct. Mater.* **2003**, *13*, 118–126.
(38) Hulea, V.; Brunel, D.; Galarneau, A.; Philippot, K.; Chaudret, B.; Kooyman, P. J.; Fajula, F. *Microporous Mesoporous Mater.* **2005**, *79*, 185–194.
(39) Pelzer, K.; Philippot, K.; Chaudret, B.; Meyer-Zaika, W.; Schmid, G. *Z. Anorg. Allg. Chem.* **2003**, *629*, 1217–1222.
(40) Duteil, A.; Queau, R.; Chaudret, B.; Mazel, R.; Roucau, C.; Bradley, J. S. *Chem. Mater.* **1993**, *5*, 341–347.

obtained for Ru particles stabilized by hexadecylamine (HDA) in colloidal solution.[37a]

Experimental Section

Analytical and Spectroscopic Methods. Elemental analysis was performed by the Analytical Laboratory of the Catalysis Research Center of Süd Chemie AG, Heufeld, Germany. The measurements were performed by standard protocols employing inductively coupled plasma atom emission spectroscopy (ICP-AES).

N_2 sorption measurements were performed using a Quantachrome Autosorp-1 MP instrument and optimized protocols.

FT-IR spectra were recorded on samples as KBr pellets using a Perkin-Elmer 1720x spectrometer. The samples were prepared in a glovebox (MBraun; O_2 and H_2O continuously monitored with levels below 1 ppm). KBr was dried at 300 °C and 10^{-3} mbar for 16 h prior to specimen preparation.

GC/MS measurements were performed on a Shimadzu GCMS-QP2010 instrument using standard settings for hydrocarbon separation.

All X-ray powder diffractograms were recorded on a D8 Advance Bruker AXS diffractometer (Cu Kα radiation, 1.54178 Å) in $\theta-2\theta$ geometry and with a position-sensitive detector. All powder samples were filled into glass capillaries (diameter = 0.7 mm) in the glovebox and sealed prior to the measurements.

TEM measurements were carried out at the University of Antwerp, Belgium, on a Philips CM20 microscope operating at 200 kV and at the Hahn-Meitner Institute in Berlin on a Philips CM30 instrument with an accelerating voltage up to 300 kV (all samples were prepared on Cu grids, 300 mesh, holey carbon films, under an inert gas atmosphere in a glovebox).

All XAS measurements were performed on powder samples that were prepared inside a glovebox. The absorption edge of Ru at 22 117 eV was measured at Hasylab X1 station (Hamburg, Germany). This beamline is equipped with a Si(311) double-crystal monochromator that was used to detune to 50% of the maximum intensity in order to exclude higher harmonics present in the X-ray beam. Samples were transferred from our laboratory to the synchrotron station under argon and pressed into self-supporting wafers inside an argon-filled glovebox. The wafers were encapsulated by Kapton sticky tape. Immediately preceding the recording of XAS spectra, samples were cooled rapidly to liquid nitrogen temperature. The spectra $\mu(k)$ were measured in transmission mode using ionization chambers. A thin self-supporting wafer of RuO_2 (between the second and third ionization chambers) was measured at the same time for energy calibration purposes (E_0 = 22 130 eV). Data treatment was carried out using the software package VIPER.[41] For background subtraction, a Victoreen polynomial was fitted to the pre-edge region. A smooth atomic background $\mu_0(k)$ was evaluated using smoothed cubic splines. The radial distribution function FT[$k^2\chi(k)$] was obtained by Fourier transformation of the k^2-weighted experimental function $\chi(k) = \{\mu(k) - \mu_0(k)\}/\mu_0(k)$ multiplied by a Bessel window. The k-range was chosen to be from 3.60 to 13.95. Duplicate spectra were recorded to ensure data reproducibility.

Solid-state MAS NMR spectra were recorded on a Bruker DSX 400 MHz instrument in ZrO_2 rotors (diameter = 2.5 mm) with a rotational frequency of 20 kHz. All ^{13}C MAS NMR spectra were measured applying cross-polarization (CP) pulse programs written by H.-J. Hauswald at the Analytical Chemistry Departement at the Ruhr-University Bochum and based on standard parameters. All ^2H solid-state wide-line NMR experiments were performed at the institute of Physical Chemistry of the Freie Universität Berlin at a field of 7.03 T and a ^2H resonance frequency of 46.03 MHz. An Oxford wide-bore magnet (89 mm) equipped with a room-temperature shim unit was used. The home-build three-channel spectrometer was described recently by Buntkowsky et al.[42,43] For the experiments, a home-build 5 mm ^2H NMR probe was used.[44] Low-temperature measurements were performed in a dynamic Oxford CF1200 helium flow cryostat. An Oxford ITC 503 temperature controller was used to control the temperature. The 90° pulse width was 5.5 μs. Owing to the weakness of the signal, the solid echo technique with an echo spacing of 60 μs was used to suppress artifacts from the radio frequency pulses. The repetition time of the experiments was 1 s. To acquire the deuterium powder patterns with a reasonable signal-to-noise ratio, between 6000 and 32 000 scans per spectrum were accumulated. The basic theory of solid-state ^2H NMR is well documented[45] and only briefly summarized here. A detailed discussion of its application to the study of hydrogen interacting with transition metal complexes is given in a recent review.[46] The leading interaction in solid-state ^2H NMR is the quadrupolar interaction. In high field, a pair of orientation-dependent resonance frequencies is observed:

$$\omega_{Q\pm} = \pm Q_{zz}\frac{1}{2}(3\cos^2(\vartheta - 1) - \eta\sin^2\vartheta\cos 2\phi) \qquad (1)$$

The asymmetry parameter η gives information about the shape of the electric field gradient, and Q_{zz} is a measure of the strength of the quadrupolar interaction; ϑ and φ are the azimuth and polar angles with respect to the main magnetic field $\mathbf{B}_0$. In a non-oriented powder sample, the average over all possible orientations has to be calculated by integration over the polar angles ϑ and φ, which gives rise to the well-known Pake pattern. The quadrupolar coupling constant Q_{cc} is obtained from the experiment as

$$Q_{cc} = 4/3Q_{zz} \qquad (2)$$

The parameters of the quadrupolar interaction are extracted from line-shape analysis, employing laboratory-written Matlab programs which are based on the theory of solid-state ^2H NMR described elsewhere.[47] Our Matlab program allows simulation of spectra consisting of up to eight different subspectra, taking into account effects of finite bandwidth excitation by the radio frequency pulses.

Reactants and Solvents. All manipulations and chemical reactions were conducted using Schlenk-line and glovebox techniques (Ar, H_2O, O_2 < 1 ppm) and sealed Fischer–Porter vessels (Andrews Glass, volume = 90 mL). All solvents were catalytically dried, deoxygenated, and saturated with argon using an automatic solvent purification system from MBraun. The residual water content was determined by Karl Fischer titration, exhibiting levels of 1 ppm.

Starting Materials Synthesis. Samples of MOF-5[3] and [Ru(cod)(cot)][48] were synthesized according to literature reports. The quality and the treatment under inert conditions of the activated MOF-5 material are essential for the loading experiments; therefore, details are given here. Colorless MOF-5 crystals of typically 2 mm were activated by stirring in chloroform for 12 h and careful drying and degassing at 110 °C in dynamic vacuum (10^{-3} mbar) for 16 h. Before all further manipulations, the powder was stored under an inert gas atmosphere in a glovebox. The MOF-5 material was characterized by X-ray diffraction (XRD) and standard N_2 sorption measurements at 77 K. For the XRD measurement, MOF-5 powder

(41) Klementiev, K. V. *Viper for Windows (Visual Processing in EXAFS Researches)*; freeware, available from www.desy.de/~klmn/viper.html.

(42) Buntkowsky, G.; Roessler, E,; Taupitz, M.; Vieth, M. H. *J. Phys. Chem. A* **1997**, *6*, 67–75.

(43) Gedat, E.; Schreiber, A.; Albrecht, J.; Shenderovich, I; Findenegg, G. H.; Limbach, H.-H.; Buntkowsky, G. *J. Phys. Chem. B* **2002**, *106*, 1977–1984.

(44) Wehrmann, F.; Albrecht, J.; Gedat, E.; Kubas, G. J.; Eckert, J.; Limbach, H.-H.; Buntkowsky, G. *J. Phys. Chem. A* **2002**, *106*, 1977–1984.

(45) Schmidt-Rohr, K.; Spiess, H. W. *Multidimensional Solid State NMR and Polymers*; Academic Press: London, 1994, and references therein.

(46) Buntkowsky, G.; Limbach, H.-H. *J. Low Temp. Phys.* **2006**, *143*, 55–114.

(47) Masierak, W.; Emmler, T.; Gedat, E.; Schreiber, A.; Findenegg, G. H.; Buntkowsky, G. *J. Phys. Chem. B* **2004**, *108*, 18890–18896.

(48) Itoh, K.; Nagashima, H.; Ohshima, T.; Oshima, N.; Nishiyama, H. *J. Organomet. Chem.* **1984**, *272*, 179–88.

was filled in a glass capillary (diameter = 0.7 mm) under an inert atmosphere (glovebox) and then sealed. XRD reflections and intensities were as follows: 2θ [°] (intensity [%]) = 11.3 (6.6), 13.7 (100), 14.9 (10.6), 15.4 (51.5), 16.8 (2.4), 17.8 (10.4), 19.5 (5.7), 20.4 (20.3), 20.6 (10.4), 21.8 (2.4), 22.6 (16.1), 22.9 (5.7), 24.6 (13.7), 25.8 (4.0), 26.5 (25.0), 28.3 (6.6), 29.3 (2.6), 30.0 (16.3), 31.6 (13.9), 33.1 (3.6), 34.6 (12.1), 35.4 (5.0), 36.0 (6.2), 37.4 (5.7), 38.2 (1.5), 38.7 (1.9), 39.9 (5.4), 40.7 (1.4), 41.3 (2.8), 42.0 (3.8), 42.6 (9.9), 43.2 (6.9), 43.6 (2.6), 44.4 (2.4), 45.0 (5.0), 45.5 (1.4). The diffraction pattern fits to the XRD of MOF-5 calculated from single-crystal data.[3] The equivalent Langmuir surface area was determined to 3300 m^2/g, which is in accordance with the literature report.[12]

Preparation of [Ru(cod)(cot)]$_{3.5}$@MOF-5 (2): Infiltration of [Ru(cod)(cot)] (1) into MOF-5. In a typical experiment, a sample of 50 mg (0.065 mmol) of dry, activated MOF-5 powder and 100 mg (0.32 mmol) of [Ru(cod)(cot)] (**1**) were placed in two separate glass vials in a Schlenk tube. The tube was then evacuated (10^{-5} mbar; turbo molecular pump) for 10 min, sealed, and kept at 30 °C for 6 days in static vacuum. A yellow composite material denoted as [Ru(cod)(cot)]$_{3.5}$@MOF-5 (**2**) was obtained and stored in the glovebox afterward. Yield: 123 mg (98.5% based on Ru). Elemental analysis calculated for [Ru(cod)(cot)]$_{3.5}$@MOF-5 (wt %): Ru, 18.8; Zn, 13.9; C, 51.2; H, 4.8 (O, 11.3 calculated from difference to 100%). Found: Ru, 18.7; Zn, 14.2; C, 51.1; H, 4.7 (O, 11.3 calculated from difference to 100%). IR: $\tilde{\nu}_{max}$ (KBr, cm^{-1}) 3008 (vw), 2964 (vw), 2923 (w), 2866 (w), 2817 (w), 1969 (w), 1603 (s), 1506 (m), 1432 (m), 1396 (s), 1336 (vw), 1321 (w), 1162 (w), 1069 (w), 1027 (w), 887 (w), 831 (w), 746 (m). ^{13}C MAS NMR: δ (ppm) 175.3 (COO MOF-5), 138.5 (**C**(COO) MOF-5), 131.3 (C_6H_4 MOF-5), 101.4 (C olefinic cot), 99.1 (C olefinic cot), 76.7 (C olefinic cot), 70.1 (C olefinic cod), 33.7 (C aliphatic cod), 31.6 (C aliphatic cot).

Hydrogenolysis of [Ru(cod)(cot)]$_{3.5}$@MOF-5 (2) at Mild Conditions. A 50 mg sample of the inclusion compound [Ru(cod)(cot)]$_{3.5}$@MOF-5 was placed in a glass tube and exposed to a stream of pure H_2 gas (1 sccm, 99.999%) at 25 °C for 30 min. A fast color change from yellow to dark brown was observed. Yield: 48 mg. Elemental analysis (wt %): Ru, 19.2; C, 49.2; H, 5.2 (O, 26.4 calculated from difference to 100%). IR: $\tilde{\nu}_{max}$ (KBr, cm^{-1}) 2922 (w), 2854 (w), 1606 (s), 1508 (m), 1432 (m), 1396 (s), 1322 (vw), 1293 (vw), 1262 (vw), 1158 (vw), 1106 (vw), 1020 (w), 884 (w), 824 (w), 746 (m). ^{13}C CP-MAS NMR: δ_C (ppm) 177.5 (COO, η^6-terephthalate), 175.0 (COO MOF-5), 136.8 (**C**(COO) MOF-5), 130.5 (C_6H_4 MOF-5), 91.8 (**C**(COO) η^6-terephthalate), 81.4 (C_6H_4 η^6-terephthalate), 68.1 (C olefinic η^4-cod), 33.4 (C aliphatic η^4-cod), 27.3 (cyclooctane).

Preparation of Ru@MOF-5 (4): Quantitative Hydrogenolysis of [Ru(cod)(cot)] inside MOF-5. A 100 mg (0.054 mmol) sample of the inclusion compound [Ru(cod)(cot)]$_{3.5}$@MOF-5 was placed in a Fischer–Porter bottle and evacuated for 5 min (dynamic vacuum, 10^{-2} mbar). The bottle was then filled with 3 bar of H_2 gas (99.999%) at 25 °C and heated to 150 °C for 48 h. A color change from yellow to brown was observed within the first 15 min. Some slight further darkening was visible during the treatment. After the sample cooled to room temperature, H_2 was removed in dynamic vacuum (10^{-3} mbar, 15 min), and thereafter the bottle was refilled with Ar (1 mbar). Yield: 61 mg (0.054 mmol, 100%). Elemental analysis (wt %) calculated for Ru$_{3.5}$@MOF-5: Ru, 31.5; Zn 23.3; C, 25.7; H, 1.08 (O, 18.4 calculated from difference to 100%). Found: Ru, 30.6; Zn, 23.1; C, 25.5; H, 1.06 (O, 19.7 calculated from difference to 100%). IR: $\tilde{\nu}_{max}$ (KBr, cm^{-1}) 1576 (s), 1505 (m), 1390 (s), 1259 (w), 1176 (w), 1153 (w), 1095 (w), 1017 (w), 878 (w), 829 (w), 810 (w), 745 (m). ^{13}C MAS NMR: δ (ppm): 175.1 (COO MOF-5), 136.9 (**C**(COO) MOF-5), 130.6 (C_6H_4 MOF-5).

Deuterium Adsorption at Ru@MOF-5 (4): Sample Preparation for Solid-State ^{2}H NMR Measurements. A 200 mg sample of Ru@MOF-5 (**4**) was placed in an NMR tube and evacuated for 15 min (10^{-7} mbar, turbo molecular pump). Subsequently, 1 bar of D_2 gas was added at 25 °C for 1 h. The D_2 gas was then removed in vacuo (10^{-7} mbar), and the sample was evacuated for 5 min more before the NMR tube was flame-sealed.

CO Adsorption at Ru@MOF-5 (4) for FT-IR Measurements. A 50 mg sample of Ru@MOF-5 was placed in a Fischer–Porter bottle and evacuated for 5 min (10^{-3} mbar, oil pump). The material was then treated with 1 bar of CO for 30 min at 25 °C in the sealed bottle. Afterward, the gas was removed in vacuo (10^{-3} mbar), the sample was introduced to a glovebox immediately, and a KBr pellet for FT-IR measurements was prepared inside the box. IR: $\tilde{\nu}_{max}$ (KBr, cm^{-1}) 2922 (vw), 2854 (vw), 2000 (m), 1890 (m), 1590 (s), 1506 (m), 1390 (s), 1310 (m), 1250 (vw), 1153 (vw), 1018 (vw), 882 (vw), 824 (vw), 811 (vw), 781 (vw), 745 (m).

Oxidation of Benzyl Alcohol Using Oxidized Ru@MOF-5 (4) as Catalyst. A 20 mg (0.011 mmol) sample of Ru@MOF was exposed to a stream of 4 vol % O_2 diluted in argon (1 sccm) at room temperature for 30 min. The powder was then introduced into a Schlenk tube and suspended in 5 mL of toluene, and 0.1 mL of benzyl alcohol was added. The solution was saturated with O_2 and stirred for 48 h at 80 °C. The suspension was then filtered, and the filtrate was analyzed by GC/MS.

Hydrogenation of Benzene Using Ru@MOF-5 (4) as Catalyst. A 50 mg (0.011 mmol) sample of Ru@MOF-5 was placed in a Fisher-Porter bottle, and 0.7 mL of benzene (7.8 mmol) was added. After short evacuation, 3 bar of H_2 gas was added, and the mixture was heated to 75 °C for 20 h. After 20 h, 1.43 bar of H_2 was consumed; prolonged heating does not lead to additional gas consumption. The reaction mixture was investigated by ^{1}H NMR.

Results and Discussion

Loading of MOF-5 with [Ru(cod)(cot)]. For the synthesis of ruthenium nanoparticles inside MOF-5, we selected [Ru(cod)(cot)] (**1**) as precursor. This compound has successfully been used before as precursor for surfactant-stabilized Ru colloids.[37a,c,40,49,50] It readily decomposes under hydrogen pressure in solution to give Ru(0) and cyclooctane as the only byproduct, resulting from hydrogenation of the olefin ligands catalyzed by Ru(0). In addition, **1** can be sublimed without decomposition at 30 °C and 10^{-5} mbar. It is known that **1** undergoes irreversible thermal isomerization when exposed to temperatures above 60 °C in solution.[51] The loading experiment was performed in static vacuum (10^{-5} mbar) at 30 °C for 6 days in order to ensure adsorption equilibrium and a homogeneous distribution of the Ru complex throughout the MOF-5 microcrystals at these conditions. Upon loading with **1**, the MOF-5 powder turned from off-white to yellow-orange. In order to demonstrate the inclusion of the precursor inside the MOF-5 pores, loading experiments with larger, millimeter-sized single crystals were performed as well. When the loaded crystals were cut open, the typical yellow-orange color of **1** appeared to be homogeneously distributed over the cross section (Figure 1, left).

The ^{13}C MAS NMR spectrum of the inclusion compound [Ru(cod)(cot)]$_{3.5}$@MOF-5 (**2**) is given in Figure 2a (top). The carbon resonance signals of the bdc moiety of MOF-5 were found at 175.3 (COO), 136.5 (*C*(COO)), and 131.3 ppm (C_6H_4), which nicely match the signals of pure MOF-5. The characteristic signals of [Ru(cod)(cot)] (**1**) were clearly observed at 101.4,

(49) Tristany, M.; Chaudret, B.; Dieudonne, P.; Guari, Y.; Lecante, P.; Matsura, V.; Moreno-Manas, M.; Philippot, K.; Pleixats, R. *Adv. Funct. Mater.* **2006**, *16*, 2008–2015.
(50) Vidoni, O.; Philippot, K.; Amiens, C.; Chaudret, B.; Balmes, O.; Malm, J.-O.; Bovin, J.-O.; Senoq, F.; Casanove, M.-J. *Angew. Chem., Int. Ed.* **1999**, *38*, 3736–3738.
(51) Pertici, P.; Vitulli, G.; Paci, M.; Porri, L. *J. Chem. Soc., Dalton Trans.* **1980**, *10*, 1961–1964.

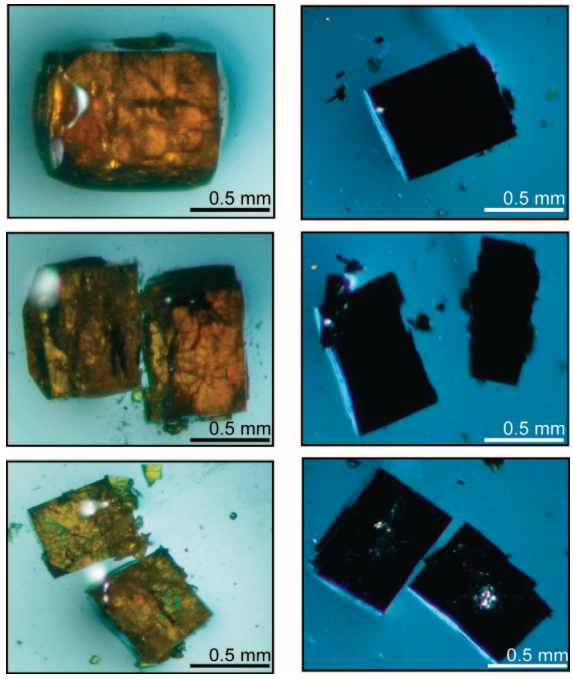

Figure 1. Images of millimeter-sized MOF-5 crystals after loading with Ru(cod)(cot) before (left) and after (right) treatment with H_2. The presented crystals on the left and the right side stem from the same loading experiment with **1**. One of them (right) was then treated with H_2. In order to show the macroscopically uniform distribution of the precursor and the Ru nanoparticles after hydrogenolysis, the crystals were cut (middle) and turned to examine the cross section (bottom).

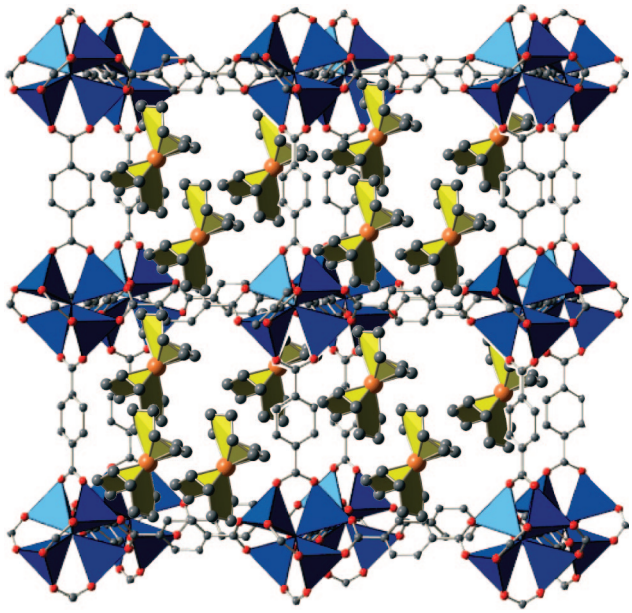

Figure 2. Model of the inclusion compound $[Ru(cod)(cod)]_{3.5}$@MOF-5 (**2**). The exact distribution of the precursor molecules over the cavities is not known.

99.1, 76.7, and 31.6 ppm for the cot ligand and 70.5 and 33.7 ppm for the cod ligand, which stem from the intact Ru complex. This is in good accordance to the literature-known ^{13}C resonances of [Ru(cod)(cot)],[51] confirming the unchanged nature of the intercalated Ru precursor. Interestingly, the adsorbed precursor molecules exhibit the same number of signals and very similar chemical shifts in the ^{13}C MAS NMR as in the conventional solution ^{13}C NMR as reference (in C_6D_6).[51] In

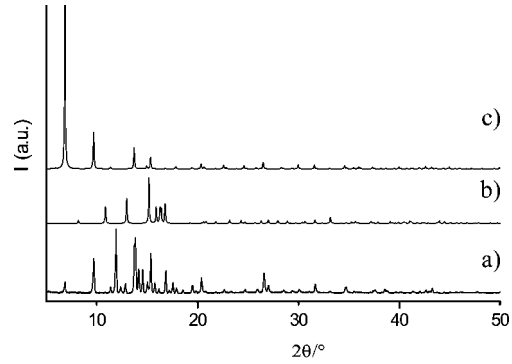

Figure 3. X-ray powder diffractograms of (a) $[Ru(cod)(cot)]_{3.5}$@MOF-5 (**2**), (b) [Ru(cod)(cot)] (calculated from the single-crystal structure[56]), and (c) empty MOF-5.

contrast, a sample of pure solid microcrystalline [Ru(cod)(cot)] reveals 16 different signals for all the carbon atoms of the cod and cot ligands in the ^{13}C MAS NMR measurement (see Supporting Information), which is in agreement with the absence of molecular symmetry in the solid state due to the crystal packing effects and the very reduced molecular mobility and conformational flexibility. But inside the MOF-5 cavities, complex **1** is apparently fluxional and mobile. It behaves almost as in solution! Thus, the ^{13}C NMR data rule out the presence of a physical mixture of the solid precursor with the MOF-5 host material. In fact, **1** is "dissolved" into MOF-5. This is quite similar to the observations for other materials of the type $[precursor]_n$@MOF-5 that we described previously and cited above.[23] In addition to the ^{13}C MAS NMR spectrum, intercalation of the precursor was also confirmed by FT-IR spectroscopy (see Supporting Information). From elemental analysis, the number of [Ru(cod)(cot)] molecules per MOF-5 formula unit was determined to 3.5 ± 0.1. This value seems to be the saturation loading at the given conditions, which was checked by variation of the amount of precursor. MOF-5 exhibits two types of cavities with different van der Waals pore diameters of 15.1 (cavity A) and 11.0 Å (cavity B), caused by the tilted bdc linkers, and pore volumes of 0.61 and 0.54 cm^3/cm^3, respectively.[3] Therefore, the number of caged molecules in each type of cavity is not necessarily the same. This effect has been reported and discussed previously on the basis of the structural characterization of $[(\eta^5\text{-}C_5H_5)_2Fe]_7$@MOF-5. In that case, the caged ferrocene molecules form an ordered superstructure with an 8:6 distribution of the A and B cavities of the MOF-5, which leads to a total of 56 ferrocene molecules per elementary cell of MOF-5 containing four A and four B cavities.[52] Hence, we suggest that the included [Ru(cod)(cot)] molecules are also distributed over the A and B cavities in a so-far unknown fashion, resulting an average loading of 3.5 molecules per formula unit. Figure 2 intends to illustrate this situation in a qualitative way, which certainly does not reflect the actual distribution.

The powder X-ray diffraction (PXRD) diagram of [Ru(cod)(cot)]$_{3.5}$@MOF-5 (**2**) is given in Figure 3a (bottom). It clearly shows the two prominent reflections of MOF-5 at $2\theta = 13.7°$ and 15.4° in the same intensity ratio as in pure activated (Ar-loaded) MOF-5, pointing at an intact host material. The decrease of the overall reflection intensity with respect to the parent, empty MOF-5 is a consequence of the inclusion of guest

(52) Kim, H.; Chun, H.; Kim, G.-H.; Lee, H.-S.; Kim, K. *Chem. Commun.* **2006**, *26*, 2759–2761.

molecules in the framework and has been well studied for zeolites and mesoporous silica materials.[53,54] In the PXRD diagram of **2**, the intensities of the reflections at 6.9° and 9.7° are inverted compared to the diagram of pure MOF-5 (Figure 3c). This corresponds to the loading of the MOF-5 pores with guest molecules.[55] The XRD of **2** also exhibits new reflections, mainly between $2\theta = 10°$ and 20°, with the most prominent new reflection at 13.8°. These reflections presumably result from some sort of ordering of the caged [Ru(cod)(cot)] in MOF-5. Clearly, the XRD of the composite is not a simple superposition of the XRD patterns of [Ru(cod)(cot)] (Figure 3b) and MOF-5 (Figure 3c). Obviously, the space confinement induced by the MOF-5 host and the preferred adsorption sites have an influence on the packing of [Ru(cod)(cot)] in the cavities, as found for $[(\eta^5\text{-}C_5H_5)_2Fe]_7$@MOF-5.[52] Thus, the packing of the [Ru(cod)(cot)] molecules inside the MOF-5 cannot resemble its solid-state structure as a pure compound. To date, we have not been able to obtain a satisfying single-crystal structure of the inclusion compounds $[Ru(cod)(cot)]_n$@MOF-5 ($n \leq 3.5$). It is noteworthy that, in the case of $[(\eta^5\text{-}C_5H_5)_2Fe]_7$@MOF-5, the single-crystal structure was determined only by using synchrotron radiation to measure a sufficient number of the (weak) superstructure reflexes of the guest molecules. In our case, one additional problem may be a nonsaturated loading of MOF-5 with the [Ru(cod)(cot)] throughout the microcrystals, which leads to an increased disorder of the rather mobile guest molecules. A similar observation was made for $[(\eta^5\text{-}C_5H_5)_2Fe]_n$@MOF-5 with $n < 7$.[23] However, the attempts to rigorously ensure thermodynamic equilibrium and a maximum loading at higher temperatures led to isomerization of **1** inside the MOF-5 matrix, as shown by ^{13}C MAS NMR (see Supporting Information). An even greater disorder of the intercalated molecules resulted. Nevertheless, all reflections observed in the X-ray powder diffractogram of **2** could be indexed by applying the same tetragonal space group. To date, only preliminary values for the cell constants have been found, and these are currently under refinement (i.e., the exact space group has still to be determined). Since pure MOF-5 crystallizes in a cubic space group, this difference provides evidence for a significant distortion and symmetry change of the MOF-5 framework itself, induced by intercalation of the guest molecules. In fact, **2** can be described as one single new phase. So far, this has not been observed for MOF-5, but similar changes of the framework symmetry upon guest inclusion are well known for MIL materials.[9,10] A detailed Rietveld analysis of **2** is currently underway and will be the topic of a future publication. Although the elucidation of the ordering of caged organometallic molecules inside the MOF matrices certainly warrants attention, the system $[Ru(cod)(cot)]_n$@MOF-5 is possibly not the best study object for that purpose because of its chemical lability. Yet, ^{13}C MAS NMR and FT-IR spectroscopy as well as XRD data prove the inclusion of intact precursor molecules into an intact MOF-5 host matrix.

Caging Effects of the Hydrogenolysis of $[Ru(cod)(cot)]_{3.5}$@MOF-5 (2) at Mild Conditions. Following the standard recipes for the preparation of Ru nanoparticles using [Ru(cod)(cot)] (**1**) as precursor in solution, the bright yellow-orange material

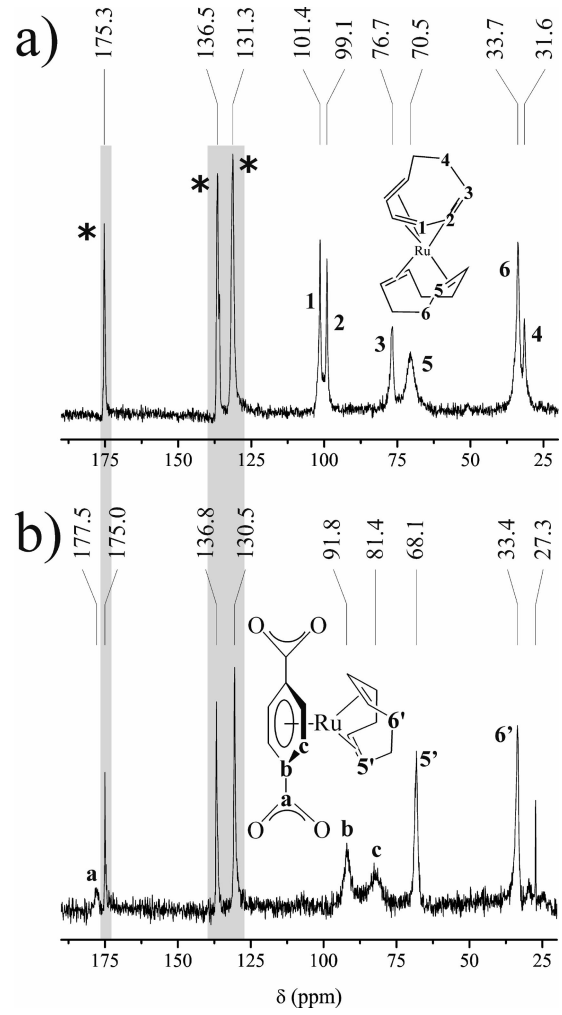

Figure 4. ^{13}C MAS NMR spectra of $[Ru(cod)(cot)]_{3.5}$@MOF-5 (**2**) before (a) and after (b) hydrogenolysis in 1 sccm H_2, 25 °C, 30 min. Signals of the framework MOF-5 are shaded. The carbon signals of MOF-5 are marked with asterisks.

$[Ru(cod)(cot)]_{3.5}$@MOF-5 (**2**) was exposed to a stream of hydrogen (1 bar, 1 sccm) at 25 °C for 30 min. A dark brown pyrophoric powder (**3**) was obtained, already indicating decomposition of **1** to Ru(0). The resulting ^{13}C MAS NMR spectrum (Figure 4b, bottom) showed the characteristic signals for the MOF-5 matrix (shaded areas in Figure 4), but five additional signals were observed, too. When comparing the ^{13}C MAS NMR of the composite **2** *before* (Figure 4a) and *after* hydrogenolysis (Figure 4b) at room temperature, it is evident that these additional signals are not derived from remaining, unchanged **1**. The resonances of the cot ligand have completely disappeared. The three broad signals at 177.5 (COO), 91.8 (*C*(COO)), and 81.4 ppm (C_6H_4) are assigned to a more rigid and now Ru-coordianted (η^6 fashion) bdc linker, and the two narrower signals at 66.1 and 33.4 ppm are assigned to the more fluxional η^4-coordinated cod ring at the Ru (Figure 4b). A signal at 27.3 ppm stems from cyclooctane as a byproduct of hydrogenolysis of **1**, which was not fully desorbed prior to the NMR experiment. Therefore, it is reasonable to suggest the coordination of a 12-electron [(cod)Ru(0)] fragment at the arene moiety of the bdc linker to form a typical 18-electron [(η^6-arene)Ru(cod)] complex in order to explain these NMR data. This assignment is in full accordance with known arene/cot exchange reactions taking place when **1** is treated with hydrogen

(53) Sauer, J.; Marlow, F.; Spliethoff, B.; Schuth, F. *Chem. Mater.* **2002**, *14*, 217–224.
(54) Marler, B.; Oberhagemann, U.; Vortmann, S.; Gies, H. *Microporous Mesoporous Mater.* **1996**, *6*, 375–383.
(55) Hafizovic, J.; Bjorgen, M.; Olsbye, U.; Dietzel, P. D. C.; Bordiga, S.; Prestipino, C.; Lamberti, C.; Lillerud, K. P. *J. Am. Chem. Soc.* **2007**, *129*, 3612–3620.
(56) Frosin, K. M.; Dahlenburg, L. *Inorg. Chim. Acta* **1990**, *167*, 83–89.

(1 bar) in the presence of arenes to yield [(η^6-arene)Ru(cod)], which are quite stable to hydrogen at lower temperatures (<50 °C).[57–59] The mild conditions (25 °C) of the treatment with H_2 (1 bar) obviously do not lead to a full splitting of the olefin ligands by hydrogenolysis. It is generally assumed that the hydrogenolysis mechanism of **1** in solution starts with hydrogenolysis of the cot ligand, releasing the [Ru(cod)] fragment which can be trapped by suitable ligands.[57,59] It is evident that not all bdc linkers of the framework are coordinated by [Ru(cod)], since the original MOF-5 signals are clearly detected and Ru nanoparticles are formed in parallel (see below). In fact, the obtained material has to be denoted as {[Ru(cod)]/Ru}@MOF-5 (**3**), with the total molar content of Ru being unchanged as compared with **2**, of course. Further details on the characterization of the obtained material **3**, including TEM and XAS studies, are given in the Supporting Information. We attempted a ligand-exchange reaction of **1** with dimethyl terephthalate (as model for the bdc linker) under 1 bar H_2 in solution. But even in the case of a large excess of dimethyl terephthalate with respect to [Ru(cod)(cot)] (40:1), only quantitative formation of a black Ru metal precipitate was observed. Interestingly, there are no reports in the literature on molecular complexes of the [(cod)Ru] fragment with terephtalic acid or its derivatives.

Taking these comparisons together, we conclude that the observed *trapping* of a significant fraction of the Ru in the form of [Ru(cod)] species coordinated at the bdc linkers is an indication of a caging effect on the kinetics of the hydrogenolysis of [Ru(cod)(cot)] *inside* MOF-5. Obviously, the coordination of the reactive intermediate [Ru(cod)] at the bdc linkers effectively competes with the hydrogenolysis and diffusion of [Ru(cod)(cot)] to yield Ru particles. A similar trapping has not been observed for the related Cu@MOF-5 and Pd@MOF-5 which were derived from the hydrogenolysis of [CpCu(PMe_3)] and [CpPd(η^3-C_3H_5)], possibly because of the absence of stable η^6-arene complexes of Cu(0) and Pd(0).[21] The diffusion of caged molecules is affected by the particular environment of the host and is also dependent on the loading. These effects have been recently analyzed in detail for the diffusion of benzene inside MOF-5.[60] The growth of Ru nanoparticles of more than 100 Ru atoms (see below) via the hydrogenolysis of isolated [Ru(cod)(cot)] molecules is likely to follow a diffusion-limited kinetics which may be slowed to some extent inside the solid matrix MOF-5 as compared with conditions in solution. On the other hand, reactive intermediates, such as [Ru(cod)], may be stabilized by caging effects in some way, and reaction paths may be altered as has been shown for a number of cases, including the trapping of the reactive 16-electron complex [CpRu(cod)$^+$] inside a tetrahedral, negatively charged metal−organic polyhedron, $[Ga_4L_6]^{12-}$.[61] Very recently, the functionalization of bdc linkers in MOF-5 with the $Cr(CO)_3$ fragment and photo-induced ligand-exchange reactions of these species were reported.[62] We particularly refer to these latter examples as references for caging effects on organometallic species inside metal−organic hosts.

(57) Pertici, P.; Vitulli, G.; Lazzaroni, R.; Salvadori, P.; Barili, P. L. *J. Chem. Soc., Dalton Trans.* **1982**, *6*, 1019–1022.
(58) Pertici, P.; Simonelli, G.; Vitulli, G.; Deganello, G.; Sandrini, P.; Mantovani, A. *J. Chem. Soc., Chem. Commun.* **1977**, *4*, 132–133.
(59) Bodes, G.; Heinemann, F. W.; Jobi, G.; Klodwig, J.; Neumann, S.; Zenneck, U. *Eur. J. Inorg. Chem.* **2003**, 281–292.
(60) Amirjalayer, S.; Tafipolski, M.; Schmid, R. *Angew. Chem., Int. Ed.* **2007**, *46*, 463–466.
(61) Fiedler, D.; BergmanR. G.; Raymond, K. N. *Angew. Chem., Int. Ed.* **2006**, *45*, 745–748.
(62) Kaye, S. S.; Long, J. R. *J. Am. Chem. Soc.* **2008**, *130*, 806–807.

Quantitative Hydrogenolysis of [Ru(cod)(cot)]$_{3.5}$@MOF-5 (2) To Yield Ru@MOF-5 (4). a. Synthesis and Analytical Characterization. In order to achieve quantitative hydrogenolysis of [Ru(cod)(cot)]$_{3.5}$@MOF-5 (**2**), treatment with 3 bar H_2 at 150 °C for a surprisingly long period of 48 h is required. After removal of all volatile byproducts (i.e., cyclooctane, as confirmed by GC/MS of the condensables), the resulting black powder, denoted as Ru@MOF-5 (**4**), revealed only the characteristic resonances of the intact MOF-5 in the ^{13}C MAS NMR. FT-IR spectra proved the absence of hydrocarbon impurities, matching the reference data of MOF-5, too. In addition, no hydrogenated bdc linkers could be detected in the ^{13}C NMR or FT-IR spectrum of **4** (see Supporting Information). From the type I isotherms of the N_2 sorption measurements of the composite, an equivalent Langmuir surface area of 860 $m^2\ g^{-1}$ was calculated. The decrease of the surface area corresponds to the embedding of Ru nanoparticles (30 wt % of Ru) in the pore system of MOF-5. A similar reduction was observed for Pd@MOF-5 and Cu@MOF-5.[21] The decrease of the surface area to approximately one-fourth the surface area of the starting material[12] could also be due to partial degradation of the crystalline long-range ordering of the framework during hydrogenolysis of the precursor at elevated temperatures. However, from XRD and TEM analysis (see below), it seems that most of the porous structure and long-range ordering remains intact. A key question is the distribution of the formed Ru particles over the MOF-5 crystallites. An enrichment of Ru at the pores near the edges of the crystallites could be possible, as one would expect the ruthenium complexes within the pores on the periphery to be reduced first, and thus these would be the initial seeds for nanoparticle nucleation. We performed hydrogenolysis experiments with individual millimeter-sized macrocrystals homogeneously loaded with **1** (Figure 1, left). After hydrogenolysis, the black crystals were cut open, and the cross section was examined by using a light microscope. The series of images on the right side of Figure 1, showing one represenative example, gives evidence of a rather uniform distribution of the black color arising from the Ru particles over the whole cross section of the crystal. This finding rules out significant enrichment of Ru particles at the edges of the macrocrystallites.

b. XAS Investigations of Ru@MOF-5 (4) and [Ru(cod)(cot)]$_{3.5}$@MOF-5 (2). The inclusion compound [Ru(cod)(cot)]$_{3.5}$@MOF-5 (**2**) and the material Ru@MOF-5 (**4**) were examined by X-ray absorption spectroscopy (XAS) in order to confirm the metallic nature of the Ru species inside the pores of MOF-5 after the decomposition of [Ru(cod)(cot)] (**1**) (Figure 5). For similar data obtained for {[Ru(cod)]/Ru}@MOF-5 (**3**), see the Supporting Information. The X-ray absorption near edge structure (XANES) of **4** (Figure 5 left, curve a) is indicative for metallic ruthenium. The curves of **4** and the reference Ru foil (curve d) overlap to a large degree; moreover, the edge-shift suggests that no oxidation of the ruthenium has taken place during sample manipulation for the ex situ XAS measurements. The amplitude of the first Ru−Ru shell in the FT (curve a) of **4** is very low when compared to that of the Ru foil. This suggests very small ruthenium particles, matching the space confinement in the MOF-5 pores. In the EXAFS (Figure 5, right) it is seen that the Ru−Ru shell (at 2.44 Å, uncorrected FT) is flanked on the left by a large shoulder (1.95 Å, uncorrected FT). In order to get some insight into the origin of this shoulder, XAS of **2** was recorded (Figure 5 left, curve b). The corresponding XANES looks strikingly different from those of both sample of **4** and the Ru foil (curve d), with a single white line and an edge

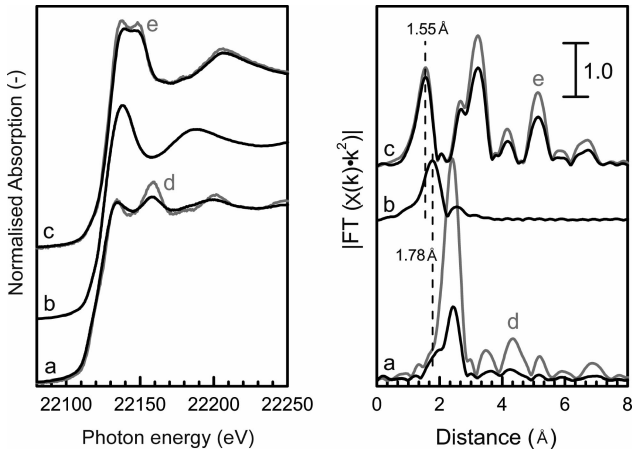

Figure 5. XANES (left) and EXAFS (right) of (a) Ru@MOF-5 (**4**), (b) [Ru(cod)(cot)]$_{3.5}$@MOF-5 (**2**), and (c) Ru-ox@MOF-5, compared to (d) Ru foil and (e) RuO_2. All data were recorded at liquid nitrogen temperature.

position of ~22125 eV. In the respective EXAFS (Figure 5 right, curve b), a peak at 1.78 Å (uncorrected FT) is likely to arise from a Ru−C bond. Modeling this peak with a single Ru−C scattering path proved unsuccessful; indeed, the Nyqist theorem prohibits fitting of many Ru−C contributions to a single peak. In the precursor **1**, many Ru−C bonds are found within the range of 2.1–2.7 Å. Right of the Ru−C peak, a smaller contribution is visible, but farther away from the central atom no higher shell structure appears in the EXAFS. On the other hand, in sample **4** (Figure 5 right, curve a), higher shell contributions matching those of the metallic state are seen. The peak position of the left-side shoulder next to the main contribution (1.8 Å, uncorrected) is comparable to that of the Ru−C contribution (1.78 Å, uncorrected) in the EXAFS of **2**, which results from the adsorbed, intact precursor molecule. In order to investigate whether this left-side shoulder may arise from unintentional partial oxidation, intentionally oxidized **4** was also analyzed by XAS measurements. A sample of **4** was exposed to a stream of 4 vol % O_2 in argon (1 sccm) for 30 min at room temperature (curve c). The XRD diagram recorded after the O_2 treatment shows the presence of the intact MOF-5 (see Supporting Information). The XANES and EXAFS of this oxidized sample are akin to those of the anhydrous RuO_2 structure.[63] The peak height in the EXAFS is slightly smaller when compared to that of the reference oxide (curve e), indicative of a smaller particle size. The long-range order of these oxide particles is manifested in the higher shells, which follow the pattern seen for RuO_2 (EXAFS). Likewise, the XANES shows the characteristic double feature associated with RuO_2, with a slightly smaller distance between the first two maxima. This is also interpreted in the light of the small particle size of the ruthenium oxide species in the MOF-5 material. From the EXAFS of the oxidized sample, it can also be concluded that the shoulder in the EXAFS of **4** does not arise from partial oxidation; i.e., there is no significant contribution of Ru−O contacts for **4**. Taking all these arguments together, we suspect that the shoulder stems from the coordination/interaction of the very small ruthenium particles with the arene carbon atoms of the MOF-5-linkers.

c. XRD and TEM Studies. XRD measurements of the Ru@MOF-5 material (Figures 6a,c) show the characteristic

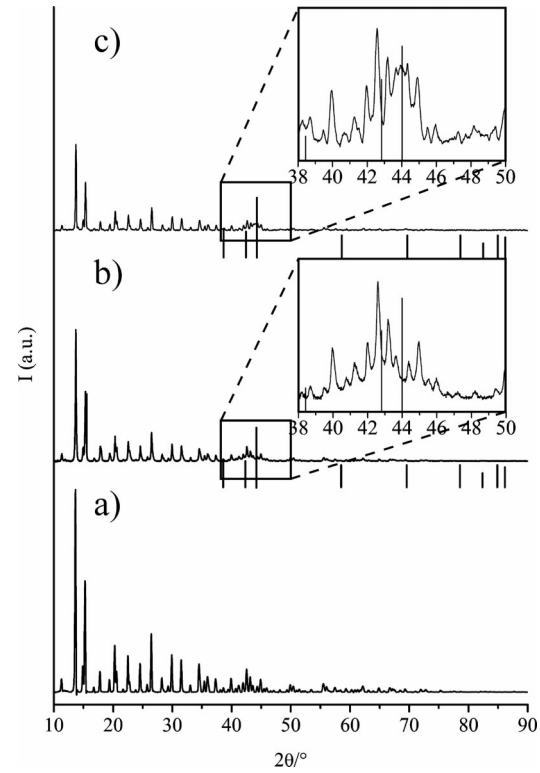

Figure 6. Powder X-ray diffraction patterns of (a) pure, activated MOF-5, (b) {[Ru(cod)]/Ru}@MOF-5 (**3**; derived by treatment of **2** with 1 sccm H_2, 25 °C, 15 min), and (c) Ru@MOF-5 (**4**; derived by treatment of **2** in 3 bar H_2, 150 °C, 48 h) (lines: Ru JPDS reference no. 6-0663). Enlargements of the region between $2\theta = 38°$ and 50° are shown as insets.

reflections of the host matrix, confirming the intact structure of MOF-5 after the precursor decomposition. By comparing the XRD data of the materials derived from **2** after hydrogenolysis at 1 bar and 30 °C and 3 bar H_2 pressure and 150 °C to the XRD pattern of pure MOF-5, an overall intensity change of the XRD reflections is visible. This finding is assigned to the higher X-ray absorption of the embedded metal particles, which has an influence on the intensities of the framework reflections as well. Similar observations have been made for loaded silica materials.[53,54] However, unlike the observation for the intercalation compound **1**, the characteristic pattern of the MOF-5 reflections is perfectly retained. No other (sharp) reflections were detected. However, the XRD diagrams of **3** and **4** exhibit a broad structure at $2\theta = 41–45°$, with a superposition of sharp MOF-5 reflections. In the case of **4**, the structure centered at $2\theta = 44.0°$ can be assigned to the (101) reflection of hexagonal close-packed Ru with an estimated full width at half-maximum of $1.5 \pm 0.2°$ (calculated by Bruker Diffrac Plus Eva 2004 software, version 10.0; see Supporting Information). In the case of **3**, the even broader structure can be assigned to an overlapping of the (001) reflection at $2\theta = 42.1°$ and the (101) reflection as above. The reason for this small but significant difference may be that prolonged hydrogenolysis at 150 °C leads to Ru particles with somewhat larger crystalline domains, as in the case of **4** as compared with **3**. However, no other reflections of metallic ruthenium were detected, which points to very small sizes of the nanocrystallites. Note that the broad structures disappear (see Supporting Information) when the material is oxidized and transformed into **4**, as discussed above in the XAS section. This finding of very broad, low-intensity reflections is in accordance with earlier studies on the formation of Ru nanoparticles in

(63) Altwasser, S.; Sulaiman Lo, R. G. A.; Liu, P.; Chao, K.; Weitkamp, J. *Microporous Mesoporous Mater.* **2006**, *89*, 109–122.

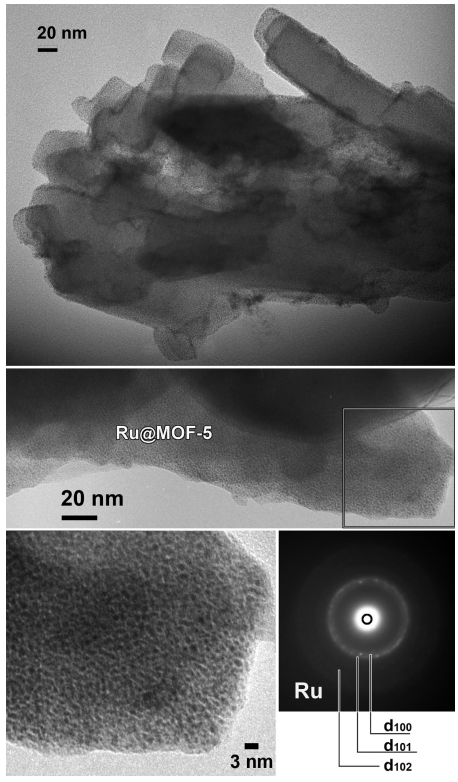

Figure 7. TEM images of Ru@MOF-5 (**4**; derived from **2** by hydrogenolysis at 150 °C, 3 bar H_2, 48 h).

porous silica materials[38] and corresponds to nanocrystalline hexagonal Ru particles in a size regime certainly below 3 nm.[64] Yet, the single broad reflection at $2\theta = 44.0°$ does not allow a more reliable estimation of the particle size by the Scherrer equation and line profile analysis, especially since there is an overlapping of two reflections at $2\theta = 42.1°$ and 44.0° and the superposition of the peaks from the host matrix. Calcination experiments on **4** up to 400 °C in vacuo led to neither decomposition of the framework nor a significant sharpening of the Ru reflections, but a rather broad peak remained (see Supporting Information).

The TEM images of Ru@MOF-5 (**4**) (Figure 7) nicely reveal the typical rectangular shapes of the MOF-5 crystallites. Although the TEM images were taken at low electron beam dosage, the ordering of the metal−organic framework is very difficult to record and visualize. Reflections of MOF-5 itself were not observed, presumably due to degradation of the material in the electron beam.[65] So far, only for the chromium terephthalate-based porous framework MIL-101 the pore structure was directly imaged and an electron diffraction pattern of the matrix could be measured.[65] The selected area electron diffraction pattern (SAED) of **4** shows the ring pattern typical for the hexagonal ruthenium structure, being broad and weak as expected from the PXRD (Figures 6b,c). Accordingly, the TEM images clearly show small Ru particles with sizes <3 nm distributed over the matrix. A close inspection of several TEM images of various sections of different reference samples and the comparison with the empty MOF-5 (see Supporting Information) material suggests that the typical size of the embedded Ru particles (imaged as black contrast dots) is around 1.5–1.7 nm. Larger particles up to 3 ± 1 nm seem to be present as well, but it is difficult to discriminate individual particles due to the two-dimensional projection of the TEM measurement. For metal nanoparticles embedded in zeolites, it is known that the particle sizes can exceed the sizes of the zeolitic cages. It was found that the porous zeolitic structure is locally distorted by the embedded particles, but the particles remain situated *inside* the porous structure.[66] We believe that this is also the case for larger Ru nanoparticles of about 3 ± 1 nm inside MOF-5. The distribution of the Ru nanoparticles throughout the MOF-5 microcrystallites was studied by tomographical TEM measurements. A preferential segregation of the Ru particles at the surface of the MOF-5 crystallites can be ruled out, which matches with the information gained from the inspection of the cross section of the Ru-loaded macrocrystals (see Supporting Information). The displayed sample exhibits a Ru content of 30 wt %. Since Ru nanoparticles in a size regime of the larger MOF cavity A (1.5 nm) are likely to consist of approximately 140–150 atoms (e.g., an ideal three-shell icosahedral model cluster is composed of 147 atoms),[67] only about 2% of all the cavities in the MOF-5 matrix would be filled with Ru particles. Due to the fluxionality and mobility of the precursor molecules within the framework, the precursor molecules and possibly small Ru clusters (nuclei) as well are able to move around different MOF-5 cavities. Upon hydrogenolysis of [Ru(cod)(cot)] (**1**), "liberated" Ru atoms from different molecules will fuse to nanoparticles, leaving some MOF cavities empty. This can also be verified by the low angle PXRD of **4** (see Supporting Information). The intensity of the reflection at 6.9° is generally assumed to correspond to the loading of MOF-5 cavities.[55] In the pure, activated MOF-5, the intensity of the reflection at 6.9° is apparently higher than the intensity of the reflection at 9.7° (Figure 3c). As discussed above, in the low-angle XRD of $[Ru(cod)(cot)]_{3.5}$@MOF-5 (**2**), the intensities of these two peaks are inverted. For **4**, the intensity decrease of the reflection at 6.9° is not as pronounced as in **2**, but a difference in intensity compared to the low-angle PXRD of pure MOF-5 is clearly detected (see Supporting Information). This is in full agreement with a non-ordered pore filling and only a small fraction of the cavities being filled with Ru nanoparticles. Interestingly, no agglomerations of larger Ru particles were detected outside the MOF-5 crystallites, which is in accordance to the XAS and XRD results (Figures 5 and 6). Note that, in the case of Au@MOF-5 prepared from $[CH_3Au(PMe_3)]$@MOF-5, much larger Au agglomerates were detected outside MOF-5.[21] This absence of larger, external Ru particles again indirectly confirms the exclusive inclusion of **1** *inside* the framework, no significant adsorption at the outer surface of the MOF-5 microcrystals, and no significant desorption or diffusion-out of **1** during the hydrogenolysis of **2**.

CO Adsorption on Ru@MOF-5 (4). The surface-accessibility and chemical nature of surfactant-stabilized metal nanoparticles has been probed by CO adsorption/desorption followed by FT-IR.[68] Several adsorption studies have been performed on Ru colloids stabilized by organic polymers in solution.[37a,40] Accordingly, a sample of the Ru@MOF-5 material (**4**) was exposed to 1 bar CO at 25 °C for 30 min. The corresponding FT-IR spectrum is shown in Figure 8. CO vibrational bands at 2000

(64) Philippot, K.; Chaudret, B. *C. R. Chim.* **2003**, *6*, 1019–1034.
(65) Lebedev, O. I.; Millange, F.; Serre, C.; Van Tendeloo, G.; Férey, G. *Chem. Mater.* **2005**, *17*, 6525–6527.
(66) Kampers, F. W. H.; Engelein, C. W. R.; van Hoff, J. H. C.; Koningsberger, D. C. *J. Phys. Chem.* **1990**, *94*, 8574–8578.
(67) Schmid, G. *Chem. Rev.* **1992**, *92*, 1709–1727.
(68) Schroeter, M. K.; Khodeir, L.; Hambrock, J.; Loeffler, E.; Muhler, M.; Fischer, R. A. *Langmuir* **2004**, *20*, 9453–9455.

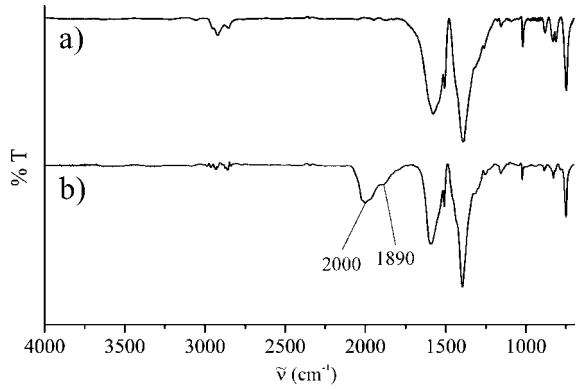

Figure 8. FT-IR spectra of (a) Ru@MOF-5 (**4**) as synthesized and (b) after 30 min of exposure to 1 bar CO.

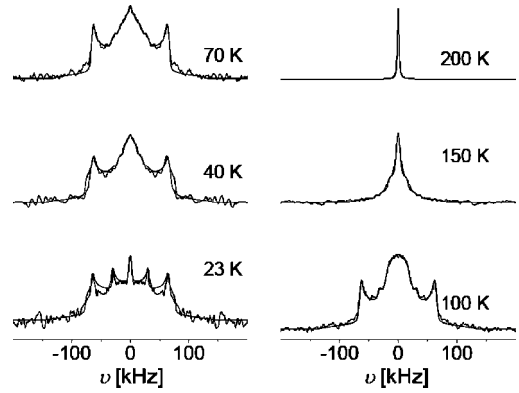

Figure 9. Experimental and simulated static solid-state ^{2}H NMR spectra of Ru@MOF-5 saturated with D_2 gas.

and 1890 cm^{-1} were observed in addition to the bands of the host material MOF-5 (compare panels a and b of Figure 8) Generally, CO bands between 2100 and 2000 cm^{-1} are assigned to CO molecules bound in a linear mode to the metal surface. Vibrational bands between 2000 and 1850 cm^{-1} are assigned to CO molecules bound in a bridging mode to adjacent metal atoms.[69] We therefore assign the CO bands at 2000 and 1890 cm^{-1} to CO in the linear and bridging positions, respectively, being adsorbed at the surface of the caged Ru particles. This finding is in accordance with CO adsorption on colloidal Ru nanoparticles. For Ru nanoparticles capped by cellulose acetate or tetranitrocellulose, also two vibrational bands were found, at 2030 cm^{-1} for linear CO and 1968 cm^{-1} for bridging CO. The particle sizes were in a similar size range of about 2 nm as compared to those for **4**.[40] Ru nanoparticles stabilized by poly(vinylpyrrolidone) (PVP) exhibit vibrational CO bands at 2040 and 1967 cm^{-1}. The average particle size was determined to be close to 1 nm, which possibly is more accurately described as a molecular Ru cluster.[70] In other studies on Ru single crystals[69] and earlier reports on Ru nanoparticles supported on oxide materials,[71] CO was found to bind only in the linear and not in the bridging mode. Recently, bridging CO was also indirectly observed on Ru nanoparticles of 1.3–2.8 nm size, supported on Al_2O_3 and SiO_2.[72,73] However, the corresponding FT-IR spectrum was more complex, dominated by vibrational CO bands for linearly bound CO on different Ru^0 and Ru^{n+} and sites. Indeed, the band for bridging the CO was very weak and only determined by fitting of the spectra.[73] Therefore, prominent bands for CO in the bridging mode, clearly distinguishable from linear bound CO, as shown in Figure 8, appear to be a unique feature of Ru colloids and the Ru nanoparticles embedded in MOF-5. The wave numbers of the vibrational bands of CO on **4** and CO on Ru colloids deviate slightly. This may be due to the different situations for the surfactants and the particle−wall interaction, respectively. Nevertheless, it is notable that **4** shows CO adsorption behavior similar to that observed for the Ru colloids capped by organic ligands such as PVP. Note that the CO adsorption on **4** is fully reversible: after evacuation (10^{-3} mbar) at 120 °C for 30 min, the FT-IR spectrum of the starting material was obtained.

Hydride Mobility of Ru@MOF-5 in Comparison with Ru Particles in Colloids. Surfactant-stabilized (e.g., HDA) Ru colloids derived from hydrogenolysis of [Ru(cod)(cot)] have been shown to be surface-covered by Ru−H species which arise from the chemisorption of dihydrogen during particle formation.[74] In addition, H/D exchange at the hydrocarbon backbone of the HDA ligands was observed as a result of the catalytic activity of the Ru particles in C−H activation reactions.[74] Inspired by these studies, we performed similar experiments with the Ru@MOF-5 material. Figure 9 compares experimental ^{2}H solid-echo NMR spectra and the simulated ^{2}H FID NMR spectra of Ru@MOF-5 (**4**) after saturation with D_2 gas in the temperature regime from 23 to 200 K. Obviously, the Ru particles promote H/D exchange with the bdc linker of MOF-5 (but without hydrogenation of the bdc). Thus, a pure sample of D_2 on **4** cannot be stabilized without partial isotope scrambling, in particular at higher temperatures. As a result of this isotope scrambling, a part of the D_2 gas inside the sample is converted to HD or H_2, and the organic ligands are partially deuterated in this experiment, resulting in the presence of C−D groups. The stoichiometry of this isotope exchange depends not only on the relative ratio of D/H but also on the possibility of contact between the bdc linker and the Ru particle surface and is not easy to interpret.[74] Note that only a fraction of the cavities is likely to be occupied by Ru particles, as discussed above. Since the measured samples contain several inequivalent deuterons, their spectra are complex superpositions of different subspectra. The shape of these spectra depends on the motional state of the deuterons and changes with temperature. At the lowest temperature of 23 K, the principal component is a broad Pake spectrum with Q_{zz} = 130–140 kHz. The second major component is a narrower Pake spectrum with Q_{zz} = 60 kHz. In addition, there is a weak narrow Lorentzian component in the center of the spectrum which corresponds to <3% of the whole intensity. Upon increasing the temperature over 40 K, to 70 and 100 K, the line shape of the narrow Pake spectrum changes strongly, indicating the presence of motions on the NMR time scale, while the broad component is practically not affected by the temperature change. This changes drastically above 100 K, however. In the spectra measured at 150 K, the broad Pake component has almost completely disappeared, except for a broad socket in the spectrum and a narrow Lorentzian line that

(69) Sheppard, N.; Nguyen, T. T. *Adv. Infrared Raman Spectrosc.* **1978**, *5*, 67–148.
(70) Bradley, J. S.; Millar, J. M.; Hill, E. W.; Behal, S.; Chaudret, B.; Duteil, A. *Faraday Discuss.* **1992**, *92*, 255–268.
(71) Dalla Betta, R. A. *J. Phys. Chem.* **1975**, *79*, 2519–2525.
(72) Chin, S. Y.; Williams, C. T.; Amiridis, M. D. *J. Phys. Chem. B* **2006**, *110*, 871–882.
(73) Chin, S. Y.; Alexeev, O. S.; Amiridis, M. D. *Appl. Catal., A* **2005**, *286*, 157–166.
(74) Pery, T.; Pelzer, K.; Buntkowsky, G.; Philippot, K.; Limbach, H.-H.; Chaudret, B. *ChemPhysChem* **2005**, *6*, 605–607.

has appeared in the center of the spectrum. Upon further increasing the temperature to 200 K, the narrow Pake spectrum also disappears, and only the central Lorentzian line is visible. The same result is also found at 300 K (not shown).

All spectra were measured at a repetition time of 1 s. This repetition time favors fast-relaxing species and suppresses slowly relaxing species. For a quantitative determination of the contributions of individual ^{2}H species, a series of experiments with variations of the recycle time, pulse width, and delay time in the solid-echo experiment has to be done in the future. Yet, the spectra shown above indicate surprisingly high mobility of the deuterons inside the MOF, even at very low temperatures, in contrast to the situation known for the HDA-stabilized Ru colloids which show a significantly reduced mobility at the same conditions. In that latter case, a reduced mobility of the deuterons was already observed at 200 K.[74] The broad component with Q_{zz} = 130–140 kHz is typical for immobile C−D groups.[47] The narrow Pake line with Q_{zz} = 60 kHz is typical for deuterons bound to ruthenium nanoparticles. For both a rigid hydride-type Ru−D and C−D bond, a nearly axial symmetric quadrupolar tensor with η close to zero is expected. Thus, we attribute the Q_{zz} = 130–140 kHz component mainly to the bdc linkers deuterated by some interaction with the Ru surface and the Q_{zz} = 60 kHz component to D_2 chemisorbed on the metal nanoparticle. If the deuterium undergoes fast reorientations, the value of the quadrupolar tensor and thus also the quadrupolar coupling constants are changed, depending on the type and speed of the motion. Thus, the line shape changes observed in the narrow Pake spectrum of the Ru−D species are also a clear indication of a high mobility of the deuterons on the Ru surface already at 40 K, while the metal−organic framework is rigid at least up to 100 K. The disappearance of this component above 100 K is not completely clear yet. It may be an indication of a starting mobility of the organic ligands, which causes very short T_2 relaxation and suppresses the signal in the echo sequence. However, a full elucidation of the observed effects will be the subject of future investigations. In conclusion, the high mobility of the deuterons on the Ru nanoparticles in MOF-5 even at 40 K hints at a rather weak interaction between the particles and the stabilizing framework, i.e., the bdc linkers, as compared with a typical surfactant such as HDA which is needed to stabilize Ru nanoparticles in colloidal solution.

Ru@MOF-5 as Catalyst for Alcohol Oxidation. According to our XAS experiments, the Ru@MOF-5 material (**4**) can be easily converted to RuO_x@MOF-5 by oxidation with diluted O_2 gas. Recent studies have shown that RuO_2 supported on Al_2O_3[30] or zeolites[29] can be used for the oxidation of a large variety of alcohols. We therefore decided to probe the catalytic activity of RuO_x@MOF in the oxidation of benzyl alcohol to benzaldehyde. The test reaction was performed in analogy to a recent report.[29] For the catalytic test, a sample of **4** was oxidized as discussed above for the XAS measurements. It was then suspended in toluene, the suspension was saturated with O_2, and benzyl alcohol was added. The reaction was then performed at 80 °C. But the observed conversion of the benzyl alcohol to benzaldehyde was only 25% (as detected by GC/MS) after 48 h. XRD examination of the material after the test reaction revealed a breakdown of the MOF-5 structure, which has lost its high porosity as well. We attribute this observation to the stoichiometric release of water during this oxidation reaction (see Scheme 1). MOF-5 is well known to be rather water-sensitive.[75] Theoretical studies by Allendorf et al. have shown that the MOF-5 structure becomes unstable above 4–6 wt % of adsorbed water.[76] Nevertheless, the expected catalytic activity of RuO_x@MOF-5 has been observed, and other water-resistant MOF support materials for the embedding of Ru and RuO_x can be selected for further studies. In addition, **4** was preliminarily tested as a catalyst in the hydrogenation of benzene (Scheme 1). The conditions were chosen according to the literature,[33] and the reaction was performed under 3 bar H_2 at 75 °C. Consumption of H_2 was followed by a pressure decrease. After 20 h reaction time, no further pressure decrease was observed, and the reaction was stopped. From ^{1}H NMR of the filtrate, the conversion of benzene to cyclohexane was detected to be approximately 25%. The PXRD diffractogram of **4** after catalysis (see Supporting Information) reveals perfectly intact MOF-5 structure as well as the typical broad Ru reflection at 44.0°. Altogether, this shows the potential of Ru@MOF-5 as a catalyst in the hydrogenation of benzene. For a complete conversion of benzene to cyclohexane, however, the ideal reaction parameters (p,T) certainly have to be adapted to the Ru@MOF-5 system.

Scheme 1. Catalytic Test Reactions with Ru@MOF-5 and RuO_2@MOF-5 as Catalyst

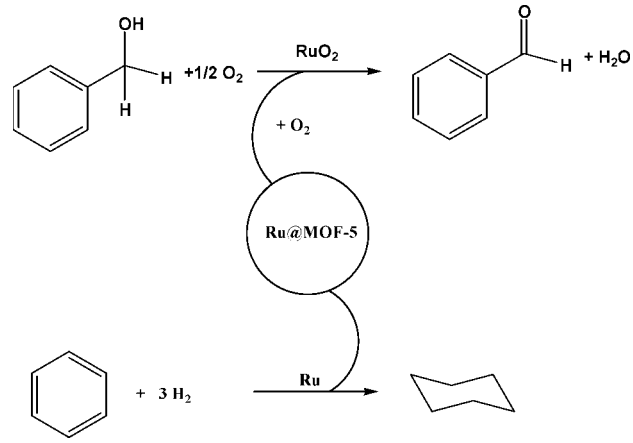

Conclusion

We have investigated the embedding of Ru nanoparticles into the otherwise unchanged metal−organic framework MOF-5. In contrast to earlier reports on the synthesis of Ru nanoparticles in porous silica,[38] we followed a two-step route. First, the well-defined inclusion compound $[Ru(cod)(cot)]_{3.5}$@MOF-5 (**2**) was derived, and then hydrogenolysis to form Ru nanoparticles inside the cavities was performed, leading to a material denoted as Ru@MOF-5 (**4**). The microstructural and chemical properties of the obtained material **4**, deduced from PXRD, XAS, TEM, and MAS NMR studies, substantiate the conceptual view of MOFs as solid solvent cages, with the organic linkers of the framework playing a role analogous to that of the solvents and/or surfactants in nanoparticle colloid chemistry. Typical sizes of the HDA-capped Ru nanoparticles sizes are between 2 and 3 nm,[37a] whereas in **4** the typical diameters of 1.5–1.7 nm for the Ru particles are smaller and almost match the dimensions

(75) Huang, L.; Wang, H.; Chen, J.; Wang, Z.; Sun, J.; Zhao, D.; Yan, Y. *Microporous Mesoporous Mater.* **2003**, *58*, 105–114.
(76) Greathouse, J. A.; Allendorf, M. D. *J. Am. Chem. Soc.* **2006**, *128*, 10678–10679.

of the MOF-5 cavities. This was deduced from the TEM images and corresponds to the qualitative data from EXAFS and XRD. EXAFS data suggest that the embedded Ru particles are in contact with the bdc linkers of the framework, which again points to quite small Ru particles. Analogies between **4** and surfactant-stabilized Ru colloids were probed by CO adsorption, H/D exchange reactions with the bdc linkers (but no hydrogenation), and the mobility of surface deuterons studied by solid-state ^{2}H NMR. Strong hints were found of a significantly higher surface mobility of the deuterons on the caged Ru particles in contrast to HDA-stabilized Ru nanoparticles. This suggests a distinctly lower interaction between the MOF-5 matrix and the embedded particles as compared with HDA as typical surfactant. HDA, as a strong σ-donor, binds more strongly to the Ru surface and therefore seems to hinder the mobility of the surface deuterons in a more pronounced way. A more detailed analysis of the NMR data and discussion of this finding are underway. Preliminary results on the catalytic activity of **4** in alcohol oxidation revealed the limitations of the water-sensitive MOF-5 host material for catalytic applications of the system metal@MOF-5. The general principles of the synthesis of Ru nanoparticles inside MOF-5 presented here can, however, be transferred to other metal−organic frameworks that are more tolerant to water, which is a subject of future studies. Last but not least, we would like to emphasize the interesting side reaction of the hydrogenolysis of [Ru(cod)(cot)] (**1**) inside MOF-5, leading to {[Ru(cod)]/Ru}@MOF-5 (**3**). This result points to possible caging effects on the reactivity of organometallic complexes inside MOFs, which warrants further studies.

Acknowledgment. The authors thank the German Research Foundation (DFG) for support within the Research Centre 558 "Metal-Substrate Interactions in Heterogeneous Catalysis". The valuable help of H.-J. Hauswald and Jun. Prof. Dr. R. Stoll from the Analytical Service Center of the Faculty of Chemistry and Biochemistry of the Ruhr-University Bochum is gratefully acknowledged in service and provision of the solid-state NMR measurements. We are grateful to Saeed Amirjalayer, M.Sc., for simulating the ^{13}C MAS NMR of [Ru(cod)(cot)]. We also thank Dr. Bernd Marler from the Department of Geosciences of the Ruhr University Bochum for help with peak indexing and Rietveld analysis. Further, the help of Dr. A. Chemseddine, Hahn-Meitner Institute Berlin, for his friendly assistance with HRTEM measurements, and Dr. A. Trautwein, Süd-Chemie AG München, for ICP/AAS measurements is gratefully acknowledged. We furthermore thank Stuart Turner from the EMAT, Physics Department, University of Antwerp, Belgium, for the 3D TEM tomography experiment. The authors acknowledge financial support from the European Union under the Framework 6 program under a contract for an Integrated Infrastructure Initiative (Reference 026019 ESTEEM). F.S. is grateful for a scholarship by the German National Academic Foundation and a fellowship by the Research School of the Ruhr-University Bochum.

Supporting Information Available: FT-IR spectrum of [Ru(cod)(cot)]@MOF-5; ^{13}C-MAS NMR spectra of [Ru(cod)(cot)], thermal isomerization of [Ru(cod)(cot)] in MOF-5, and quantitative hydrogenation of [Ru(cod)(cot)]@MOF-5 to yield Ru@MOF-5 (**4**); XAS and TEM results of hydrogenolysis of $[Ru(cod)(cot)]_{3.5}$@MOF-5 at mild conditions; PXRD, TEM measurements, tomographical TEM measurements, and temperature stability of **4**; and hydrogenation of benzene by **4**. This material is available free of charge via the Internet at http://pubs.acs.org.

JA078231U